Taylor & Francis
Taylor & Francis Group

Ship Technology Research
Schiffstechnik

ISSN: 0937-7255 (Print) 2056-7111 (Online) Journal homepage: www.tandfonline.com/journals/ystr20

Loading condition generation for the prediction of extreme vessel responses

Christopher Krause & Stefan Krüger

To cite this article: Christopher Krause & Stefan Krüger (20 Jun 2025): Loading condition generation for the prediction of extreme vessel responses, Ship Technology Research, DOI: 10.1080/09377255.2025.2518727

To link to this article: https://doi.org/10.1080/09377255.2025.2518727

SHIP TECHNOLOGY RESEARCH (SCHIFFSTECHNIK)
https://doi.org/10.1080/09377255.2025.2518727

Loading condition generation for the prediction of extreme vessel responses

Christopher Krause and Stefan Krüger

Institute of Ship Design and Ship Safety, Hamburg University of Technology, Hamburg, Germany

ABSTRACT

This paper delineates the process necessary for generating a large number of loading conditions for a seagoing cargo vessel, which are needed for an extensive analysis of the ships seakeeping behaviour. First legislative and operational limits of the floating position and its properties are described. This is followed by the chosen mathematical representation of the cargo and ballast iteration process. Results are presented for four different types of cargo vessels and concluded with an outlook on possible applications.

ARTICLE HISTORY
Received 31 March 2025
Accepted 9 June 2025

KEYWORDS
Ship operations; ship performance; ship safety; seakeeping; international maritime legislation; artificial intelligence

	Roman letters
B	Beam [m]
D	Depth [m]
GT	Gross tonnage
$\overline{GM}$	Metacentric height [m]
i	Control variable
$\overline{KM}$	Height of metacentre above origin [m]
L	Length [m]
LSW	Light ship weight [t]
m	Mass [t]
M	Moment [mt]
n	Number
T	Draught [m]
t	Trim [m]
x	Lengthwise coordinate [m]
y	Transverse coordinate [m]
z	Vertical coordinate [m]
$\vec{x}$	Shipfixed location vector [m]
	Greek letters
α	Aerial load [t/m^2]
Δ	Displacement [t]
κ	Random number within [0,1] [-]
μ	Lane load [t/m]
ξ	Tank filling [%]
	Superscripts and subscripts
AP	At after perpendicular
CG	Of centre of gravity
comp	Of weight component
des	As designed
EQI	At equilibrium
FEU	Forty-foot equivalent unit
FP	At fore perpendicular
OA	Over all
OX	At $0.5 \cdot L_{PP}$
PP	Between perpendiculars
SC	Scantling
$\hat{\cdot}$	Maximum
$\check{\cdot}$	Minimum
$\bar{\cdot}$	Mean
$\tilde{\cdot}$	Deviation
$\partial\cdot$	Gradient along $\cdot$

1. Introduction

The seakeeping behaviour of a ship is a major factor in the safety of its crew and cargo as well as for the environment. The ongoing exploitation of ship designs for an ever greater payload capacity raises the necessity for extensive analyses of the seakeeping performance. To do so, the entire range of possible loading conditions of a vessel must be known and sufficiently accounted for. The seakeeping behaviour of a particular loading condition is mainly affected by its stability and inertia. Both are influenced by the amount and location of cargo and other deadweights on board. Furthermore the stability is governed by the resulting floating position. Therefore three variables are identified: the mean draught, trim and natural roll period. The latter is a combination of the metacentric height in a seaway and the roll radius of gyration (Krause 2019). While a simple permutation of these variables would be possible, this would produce a lot of useless data points, since the occurrence of any given combination of draught, trim and roll period is highly dependent on the ship type and individual ship layout. Therefore this work uses another approach utilizing knowledge about the distribution of cargo, consumables and ballast on board. Once this process is implemented, the overall target is to use these loading conditions for the calculation of training data for use with artificial intelligence. This process is described in Krause and Krüger (2025a) and an exemplary application is documented in Krause and Krüger (2025b).

CONTACT Christopher Krause christopher.krause@tuhh.de Am Schwarzenberg-Campus 4, 21073 Hamburg, Germany

2. Theory

The range of achievable loading conditions is governed by several factors, both legislative and operational. Their effects will be described in the following.

2.1. Legislative limits

To ensure a basic level of safety in the operation of ships, the seafaring nations of the world have implemented a variety of rules through their governing body, the International Maritime Organization (IMO). The relevant sets of rules will be described now.

2.1.1. Load lines convention

The Load Lines Convention (2021) limits the maximum submersion or draught of a vessel by requiring a minimum freeboard between the deepest waterline and the freeboard deck. This draught is indicated by the load line mark, which generally must not be submerged at any time while at sea (Load Lines Convention 2021, Article 12). The underlying intent is to guarantee a minimum amount of reserve buoyancy as to ensure sufficient hydrostatic restoring forces against external effects from wind and seaway.

Further relevant requirements mandate (Load Lines Convention 2021, Annex B Reg. 1) that the structural strength of the hull girder shall be sufficient. This may be confirmed through the rules of a classification society. For this work, these requirements result in the need to check whether any loading condition exceeds the longitudinal strength of the hull girder. This will be done by calculating the internal shear forces and bending moments, which are checked against the permissible values of the particular vessel.

2.1.2. Code on intact stability

While the Load Lines Convention provides the ability to have sufficient restoring forces, the Code on Intact Stability (IS Code) (2020) gives specific requirements to the righting lever curve of any given loading condition. The assessment of these individual rules results in an envelope curve of the minimum required metacentric height for any given draught.

The occurring heel of any loading condition is not explicitly governed by the IS Code. However International Code on Intact Stability (2020, 2.5.1) mandates the master to execute good seamanship. It is derived from this that a ship shall put to sea *upright*. The lack of a clear regulation in this regard has opened an area of debate about the limits of heel. In any case if the heel exceeds the limit, water ballast may be used to mitigate this situation.

2.1.3. Safety of life at sea

The International Convention for the Safety of Life at Sea (SOLAS) (2020) stipulates further requirements for any floating position of a vessel. While the IS Code governs the stability for an intact vessel, SOLAS (2020, Part B-1) regulates the minimum requirements for cases of a damaged ship. The fulfilment of these rules yields another curve of minimum required metacentric height, which is added to the envelope curve given by the IS Code.

The occurring heel of any loading condition is not explicitly governed in SOLAS either. However SOLAS (2020, Part B-4 Reg. 20) requires the master of a passenger ship to ensure that the vessel is *upright* upon departure. This is taken as a further hint to the previously mentioned arguments on this topic.

Further SOLAS (2020, Part A-1 Reg. 3–1) also mentions the structural soundness of a vessel in similar ways to the Load Lines Convention. Therefore the same considerations apply.

2.1.4. Prevention of marine pollution

The International Convention for the Prevention of Marine Pollution from Ships (MARPOL) (MARPOL CONSOLIDATED EDITION 2022) gives limitations to the floating position of tankers. However the described work is not focused on this type of ship, therefore these regulations would only be implemented if the need arises.

2.1.5. Further guidelines

Beyond the required rules, the governing bodies have published further guidelines on the safe operation of ships. Noteworthy are the developments of second generation intact stability requirements concerning the dangers in heavy seas, both with low and excessive stability. However since these are not required as of the publication date of this work, they are not considered as a hard limit to the ships loading conditions.

2.2. Operational limits

Beyond the legislative limitations, there are several other limits that result from the need of an acceptable operation of a vessel. General guidelines on this topic may also be found in Papanikolaou (2014, p. 136–140). Since these limitations are specific to the ship and are generally not defined by a specific formula, further user input on the minimum and maximum draught amidship and at the perpendiculars is required.

2.2.1. Propulsion

A not fully submerged propeller has serious consequences for the ship performance and mechanical soundness (Ghaemi and Zeraatgar 2022). Because of ventilation the efficiency of the propeller is greatly

reduced, which leads to a higher fuel consumption. Further the propellers thrust is generated more eccentrically, which leads to higher loads and vibrations in the drivetrain as well as a higher potential for failure of the stern tube bearings. Therefore it is assumed that the floating position is trimmed so that the draught at the after perpendicular submerges the propeller blade tips.

It may also be considered that the immersion of a transom stern influences the ship resistance to a noticeable extent. However, the balance between an increase in fuel consumption and a larger transported payload varies between vessels and vessel types.

2.2.2. Steering

The manoeuvrability of a vessel is generally governed by the IMO resolution MSC.137(76). This legislation, however, only validates the requirements for a fully-laden ship without any trim. It is known that the course stability of a vessel greatly depends on the floating position, especially on the trim (Yasukawa et al. 2022). A trim towards the stern increases the course stability and somewhat reduces the turnability. On the other hand, a trim towards the bow not only increases the turnability but also increases the risk of course instability. Therefore a certain maximum bow trim may be considered as a limit to the floating position.

2.2.3. Slamming

Sections of a ship hull that have a large flare may experience slamming in seaway. Typical areas of concern are the shell plates of a transom stern and the ship bottom at the bow. Slamming on the latter is usually avoided by having a sufficient draught at the forward perpendicular (Daewoo Shipbuilding & Marine Engineering 2015, p. G7). This is therefore considered as another limit to the floating position.

3. Calculation method

The following shall delineate the implemented calculation method for generating loading conditions by picking the payload and bunker distribution by random and afterwards choosing ballast for an appropriate floating position. The described process is also visualized in Figure 1.

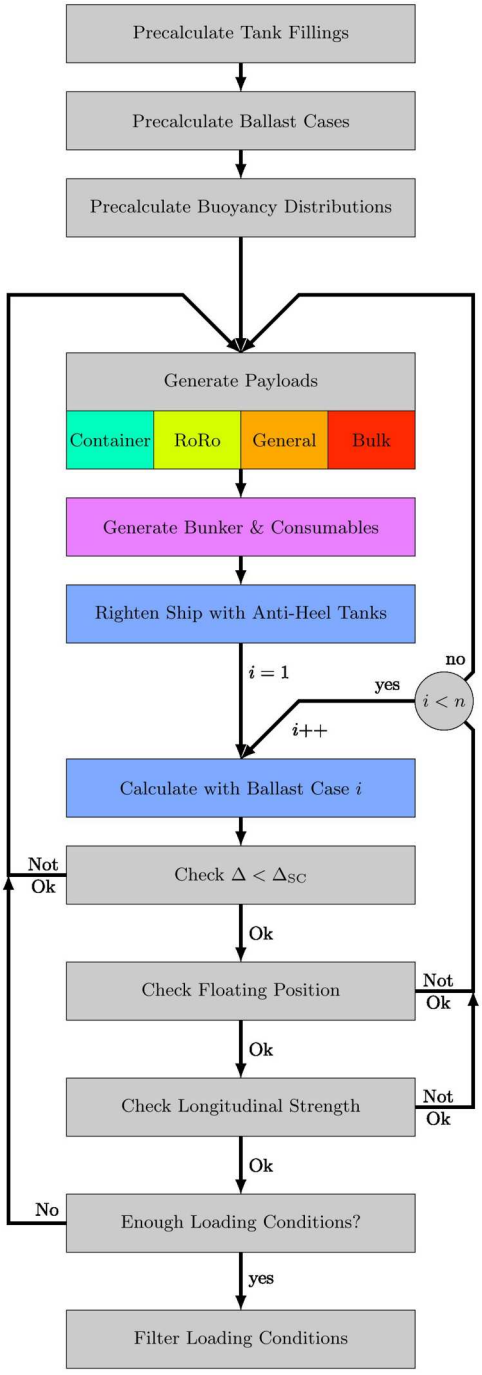

Figure 1. Flow chart of the generation process.

3.1. Preceeding ballast calculations

Since the generated loading conditions, which are drawn by random, shall, if possible, be ballasted to achieve a valid floating position, the options for ballasting must be analysed. The amount of possible ballast combinations is dependent on the number of tanks and the required filling resolution resulting in a theoretically impractically large number of combinations. In case of an exemplary ultra large container vessel with 35 ballast tanks and a filling resolution of 10% steps this number is 11^{35}. However almost all of these combinations are absolutely irrelevant for the ship operation. Therefore another approach must be implemented to find a sufficient number of practical ballast distributions. For this the question is asked, for what effect taken ballast is used. Antiheeling tanks may be used to give the vessel an upright floating position. Further ballast water in bow or stern tanks may be needed to achieve an acceptable trim. Finally ballast may be needed midships to have an overall sufficient draught, a satisfactory stability and possibly to avoid a structural overloading of

the hull girder. These ballast patterns may be found by analysing the ballast tank geometry in a three-dimensional way using two decision planes. As an initial step, the antiheel function is separated from the trim and draught, because generally specific tanks are disclosed for this. Next the center of gravity (CoG) of each filling step of each tank is calculated by using the compartmentation model of the vessel. Because the floating position of the vessel is not known at this time, no heel or trim can be considered.

Afterwards a pair of decision planes is moved throughout the vessel. These planes are generated by the shipfixed points $\vec{x}_1$, $\vec{x}_2$, $\vec{x}_3$ and $\vec{x}_2$, $\vec{x}_3$, $\vec{x}_4$ as defined by Equations (1)–(3) respectively. Both planes share the points 2 and 3 which step through L_{pp} by i_x. A step range from 0 to 20 is applied by default for this. By their y-value of $\pm 0.5 \cdot B$ they also define the orientation of the planes as normal to the xz-plane of the ship. The remaining points 1 and 4 are L_{pp} behind or ahead of the common points. All points step through the ship vertically by $z(i_z)$ which by default is setup from the base line up to $2 \cdot D_{SC}$ in $0.01 \cdot D_{SC}$ increments. The opposing gradient of the two planes is generated by the addition of a second vertical term at points 1 and 4. This addition is of cubic nature, which leads to a fine resolution for ballast cases where most double bottom tanks are filled, while also achieving cases where only bow or stern tanks are used. The control variable $i_{\partial z}$ steps through a range from $-n_{\partial z}$ to $+n_{\partial z}$ so that gradients in both directions are possible. $n_{\partial z}$ is set to 10 by default.

$$\vec{x}_1 = \begin{pmatrix} \left(\frac{i_x}{n_x} - 1\right) \cdot L_{pp} \\ 0.0 \\ \frac{i_{\partial z}^3}{n_{\partial z}^2} \cdot D_{SC} + z(i_z) \end{pmatrix} \tag{1}$$

$$\vec{x}_{2,3} = \begin{pmatrix} \frac{i_x}{n_x} \cdot L_{pp} \\ \pm 0.5 \cdot B \\ z(i_z) \end{pmatrix} \tag{2}$$

$$\vec{x}_4 = \begin{pmatrix} \left(\frac{i_x}{n_x} + 1\right) \cdot L_{pp} \\ 0.0 \\ \frac{i_{\partial z}^3}{n_{\partial z}^2} \cdot D_{SC} + z(i_z) \end{pmatrix} \tag{3}$$

For each step, all tank fillings with their CoGs below these planes are considered filled. A 3D example of this is shown in Figure 2, where the decision planes are drawn in yellow, ballast tanks in blue and their CoG as purple points. It is recognized that this procedure results in cases with a large number of partially filled tanks. This is generally avoided in ship operations, because of a stability reduction due to free surface effects. However, the impact of fluid motion while encountering seaway greatly dependent on the relation between the periods of fluid sloshing and ship motion. The former is also a function of the tank geometry and filling level. Because the fluid motion within ballast tanks is generally less than in cargo tanks, which are mostly empty or filled up because of this, it is assumed that the sum of all ballast tank effects is small. This leads to them being considered fixed masses within later seakeeping calculations.

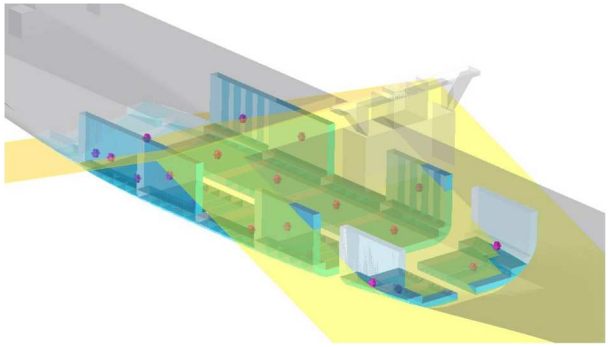

Figure 2. Exemplary application of decision planes.

Once all steps of the decision planes have been run through, some cases may have resulted in the same combination of tank fillings. They are therefore filtered for uniqueness and sorted by the total ballast mass. Examples of such ballast cases may be found in Figure 3.

3.2. Preceeding calculation of buoyancy distributions

To evaluate the internal forces of the hull girder, the distributions of weight and buoyancy along the hull must be known. Therefore the buoyancy distribution for a variety of floating positions is calculated in advance as to reduce computation time within the ballast iteration loop.

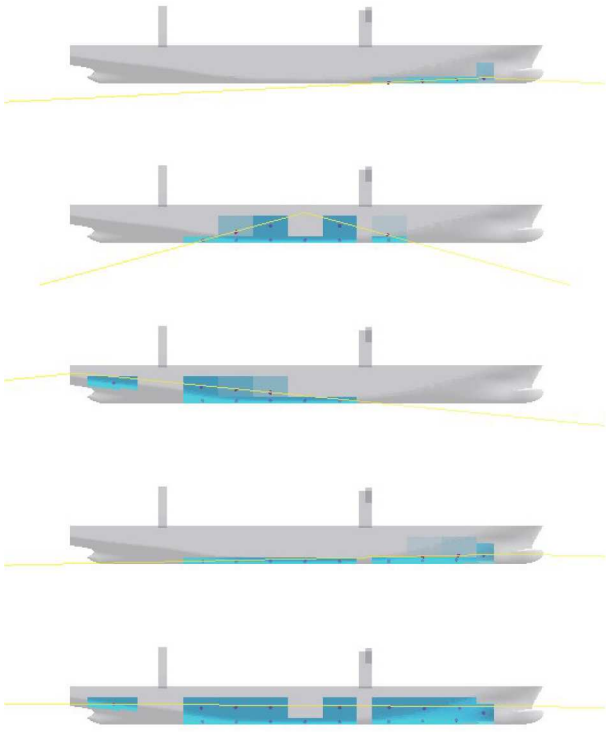

Figure 3. Examples of generated ballast cases.

3.3. Payload distribution

For the generation of payload distributions knowledge about its type, amount and location on board must be supplied by the user. With this a random distribution of each payload type is generated and their overall CoG calculated.

3.3.1. Containers

The container distribution on board is defined by bays in x-, rows in y- and tiers in z -directions. Obviously the filling of a bay is conducted bottom-up. Therefore the container distribution is generated by first drawing a mean level to which all bays are filled equally (Equation 4). Second a differential term is drawn for each bay, which defines its filling in respect to the mean (Equation 5). The filling of each individual bay is then drawn by random as a combination of the two former (Equation 6).

$$\bar{n}_{\text{tier}} = \text{nint}(\kappa \cdot \hat{n}_{\text{tier}}) \tag{4}$$

$$\tilde{n}_{\text{tier}} = \text{nint}(\kappa \cdot \min(\bar{n}_{\text{tier}}, \hat{n}_{\text{tier}} - \bar{n}_{\text{tier}})) \tag{5}$$

$$n_{\text{tier}}(i_{\text{bay}}) = \bar{n}_{\text{tier}} + \text{nint}((-1 + 2 \cdot \kappa) \cdot \tilde{n}_{\text{tier}}) \tag{6}$$

To reduce the total number of payload items, the containers of a single tier are merged across the rows into a single component. First the mean container mass is drawn by random within the range of its empty weight and maximum gross tonnage (Equation 7). Next a term of variation is drawn analogous to the bay filling (Equation 8). Finally the number of rows is taken from the container arrangement and the component mass is calculated (Equation 10).

$$\bar{m}_{\text{cont}} = \check{m}_{\text{cont}} + \kappa \cdot (\hat{m}_{\text{cont}} - \check{m}_{\text{cont}}) \tag{7}$$

$$\tilde{m}_{\text{cont}} = \kappa \cdot \min(\bar{m}_{\text{cont}} - \check{m}_{\text{cont}}, \hat{m}_{\text{cont}} - \bar{m}_{\text{cont}}) \tag{8}$$

$$m_{\text{cont,i}} = \bar{m}_{\text{cont}} + (-1 + 2 \cdot \kappa) \cdot \tilde{m}_{\text{cont}} \tag{9}$$

$$m(i_{\text{comp}}) = m_{\text{cont,i}} \cdot n_{\text{rows}}(i_{\text{bay}}, i_{\text{tier}}) \tag{10}$$

Furthermore, in-homogeneous loading of containers has to be accounted for. This results in a variation of the components CoG. For this the maximum range for the CoG deviation is calculated. First the minimum and maximum line loads of the component in y-direction according to Equations (11) and (12), as well as x-direction analogously, are computed.

$$\check{m}_{\partial y} = \begin{cases} \frac{\check{m}_{\text{cont}}}{\hat{y} - \check{y}} & 2 \cdot m_{\text{cont,i}} < \hat{m}_{\text{cont}} - \check{m}_{\text{cont}} \\ \frac{\check{m}_{\text{cont}} - 2 \cdot (\check{m}_{\text{cont}} - m_{\text{cont,i}})}{\hat{y} - \check{y}} & \text{else} \end{cases} \tag{11}$$

$$\hat{m}_{\partial y} = \begin{cases} \frac{\hat{m}_{\text{cont}}}{\hat{y} - \check{y}} & 2 \cdot m_{\text{cont,i}} > \hat{m}_{\text{cont}} - \check{m}_{\text{cont}} \\ \frac{\hat{m}_{\text{cont}} + 2 \cdot (m_{\text{cont,i}} - \check{m}_{\text{cont}})}{\hat{y} - \check{y}} & \text{else} \end{cases} \tag{12}$$

Second the CoG range is determined by Equations (13) and (14) for y and x analogously.

$$\check{y}_{\text{CG}} = \check{y} + \frac{\check{m}_{\partial y} + 2 \cdot \hat{m}_{\partial y}}{\check{m}_{\partial y} + \hat{m}_{\partial y}} \cdot \frac{\hat{y} - \check{y}}{3} \tag{13}$$

$$\hat{y}_{\text{CG}} = y_{\min} + \frac{\hat{m}_{\partial y} + 2 \cdot \check{m}_{\partial y}}{\check{m}_{\partial y} + \hat{m}_{\partial y}} \cdot \frac{\hat{y} - \check{y}}{3} \tag{14}$$

For each component, the resulting CoG is then drawn by random as defined by Equation (15) for y and x analogously.

$$y_{\text{CG}} = \check{y}_{\text{CG}} + \kappa \cdot (\hat{y}_{\text{CG}} - \check{y}_{\text{CG}}) \tag{15}$$

A variation of CoG in z-direction is not conducted, because the height of a container component in this context is generally the smallest dimension. The CoG height in respect to the container bottom edge is therefore set to the common value of 45% of its height. The dimensions of a single container unit may be defined by the user, but are considered constant. Because of this no distribution among standard height and high cube containers or TEUs and FEUs is implemented.

Repeating this procedure for all tiers and bays of the drawn filling level results in a varying distribution of the container payload.

3.3.2. RoRo cargo

The distribution of roll-on/roll-off cargo on board is defined by decks and lanes, the latter representing an individual payload component. Therefore the weight distribution of vehicles on each lane is merged into a single component. As a first step, lanes are marked for their usage by random. This is achieved by drawing one random number as the general loading level of the vessel. Then random numbers for each lane are drawn. If this second number is below the general loading level, the lane is considered in use, otherwise not. Second the weight and CoG are drawn for each lane in an analogous manner to the container payloads. However it must be mentioned that the weight of a lane is dependent on its length:

$$\mu_{\text{Lane,i}} = \check{\mu} + \kappa \cdot (\hat{\mu} - \check{\mu}), \tag{16}$$

$$m(i_{\text{comp}}) = \mu_{\text{Lane,i}} \cdot (\hat{x}_{\text{i}} - \check{x}_{\text{i}}). \tag{17}$$

The variation in CoG is drawn analogous to Equations (13)–(15). The vertical CoG, however, is assumed to be one third of the lanes clear height. Repeating this procedure for all lanes and decks in use results in a varying distribution of the RoRo payload on board the ship.

3.3.3. General cargo

The distribution of general cargo on board is defined by holds and spaces, the latter representing an individual payload component. This is mainly done to be able to distribute the cargo content of a hold onto multiple

decks, as was common on general cargo vessels before the advent of container ships. For modern vessels this function may be used for example in stepped holds of heavy lift ships. Because of the chosen division, all separate cargo items of one space are merged into a single component. First the usage of a particular space is triggered in a similar manner to RoRo payloads by a random threshold. Second the weight and CoG are drawn as it has been for containers and RoRo lanes. However, this time the weight is dependent on the space area:

$$\alpha_{\text{spac,i}} = \check{\alpha} + \kappa \cdot (\hat{\alpha} - \check{\alpha}), \tag{18}$$

$$m(i_{\text{comp}}) = \alpha_{\text{spac,i}} \cdot (\hat{x}_{\text{i}} - \check{x}_{\text{i}}) \cdot (\hat{y}_{\text{i}} - \check{y}_{\text{i}}). \tag{19}$$

The variation in CoG is drawn once again similar to Equations (13)–(15). The vertical CoG, however, is assumed to be one-third of a randomly picked item height. Repeating this procedure for all spaces and holds in use results in a varying distribution of the general cargo on board.

3.3.4. Bulk cargo

The distribution of bulk cargo on board is defined by holds taken from the compartmentation model. First the usage of a hold is determined by a random threshold. Second the content density is decided upon within the specific range of the ship. It has to be noted that dry and liquid bulk cargo are considered equivalent in this context. The filling of these cargo holds is set to full since they are generally filled up completely to avoid large free surface effects.

3.4. Bunker and consumables

The fillings of bunker and other tanks of consumables are taken from the compartmentation model and drawn random within the range:

$$\xi_{\text{bunk,i}} = 10\% + \kappa \cdot 90\%. \tag{20}$$

This results in all tanks of a particular type of consumable being partly filled and therefore having free surface effects. This is usually avoided by crews to minimize the negative effect on stability. However as previously described for ballast tanks, the sum of these effects is considered negligible and not regarded in later seakeeping calculations.

3.5. Ballast against heel

The drawn distribution of payload and consumables may result in some heel. Since ships shall put to sea upright, any heel beyond 1° is corrected by filling antiheel tanks. For small angles of heel, the moment to be compensated amounts to:

$$M_{\text{heel}} = (y_{\text{CG}} - y_{\text{CG,lim}}) \cdot \Delta. \tag{21}$$

It must be noted that the CoG and Displacement must include the effects of the current filling step of the antiheel tank. The limit of the transverse CoG is given by the metacentric height:

$$y_{\text{CG,lim}} = \sin(1^\circ) \cdot \overline{GM} = \sin(1^\circ) \cdot (\overline{KM} - z_{\text{CG}}). \tag{22}$$

The available antiheel moment for any given filling step i is

$$M_{\text{anti}} = y_{\text{CG,Tank}}(i) \cdot m_{\text{Tank}}(i). \tag{23}$$

Therefore the antiheel tank on the respective side is filled until:

$$M_{\text{anti}} \geq M_{\text{heel}}. \tag{24}$$

3.6. Ballast iteration

Once the payload and consumables have been drawn and any heel has been accounted for, the resulting floating position is computed and checked according to the limits as defined in Chapter 2. If there is a need for adjustment, an iteration loop through the list of pre-calculated ballast cases ascending in total ballast weight is commenced until a case is found that yields an acceptable floating position or the vessel is laden beyond its full-scantling limit. In the former case, the generated loading condition is saved. In the latter case, the loop for generating loading conditions is repeated.

3.7. Filtering

Once a sufficient number of loading conditions has been drawn, their distribution within a three-

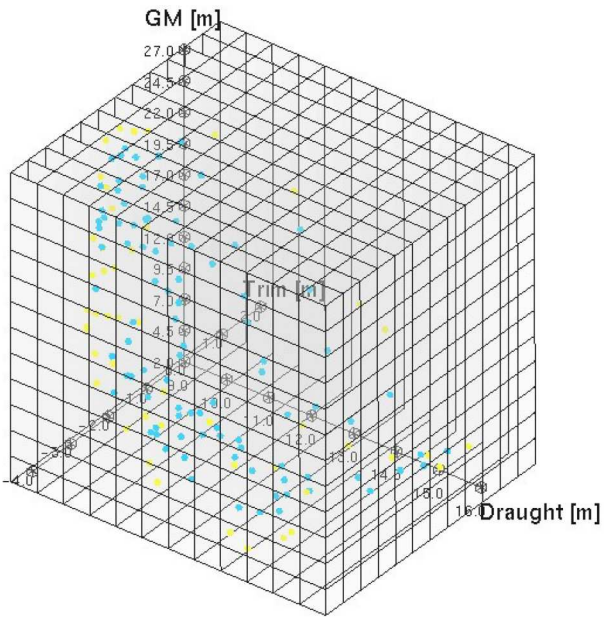

Figure 4. Exemplary cloud of loading conditions and the applied filtering cuboids.

dimensional space of draught, trim and metacentric height is random within the defined limits and is generally not homogeneous. However, the targeted usage of artificial intelligence benefits from training data, that is homogeneously distributed in the data domain. Therefore the loading condition distribution is filtered to break up local accumulations. This is done by subdividing the three-dimensional space into uniform cuboids and saving only the one loading condition, that is closest to the cuboids centre. The size of cuboids is determined by setting the extents of the domain as the centres of the outer most cuboids and uniformly dividing each dimension. This process is computed for varying total numbers of cuboids after which the user selects the final group with graphical assistance. An example of this filtering process by cuboids is visualized in Figure 4.

4. Results

To exemplify the loading condition generation process, the before described calculation method is applied to four ships. The first is an ultra large container vessel which main particulars are given in Table 1. The distribution of drawn and filtered loading conditions is visualized in 3D by Figure 5. In this and the following pictures, yellow points indicate that the particular loading condition is part of the points defining the convex envelope of the point cloud,

Table 1. ULCV main particulars.

L_{OA}	≈400 m
B	≈60 m
D	≈30 m
T_{des}	≈14.5 m
T_{SC}	≈16.0 m
LSW	≈60,000 t
Δ_{SC}	≈260,000 t
n_{TEU}	≈19,000

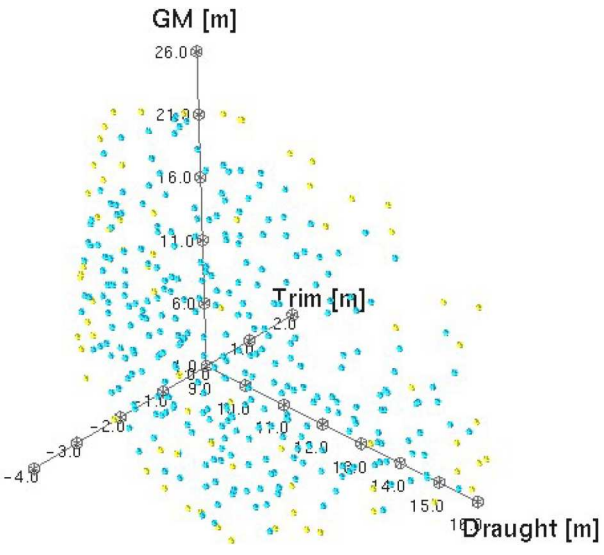

Figure 5. ULCV: 3D distribution of loading conditions.

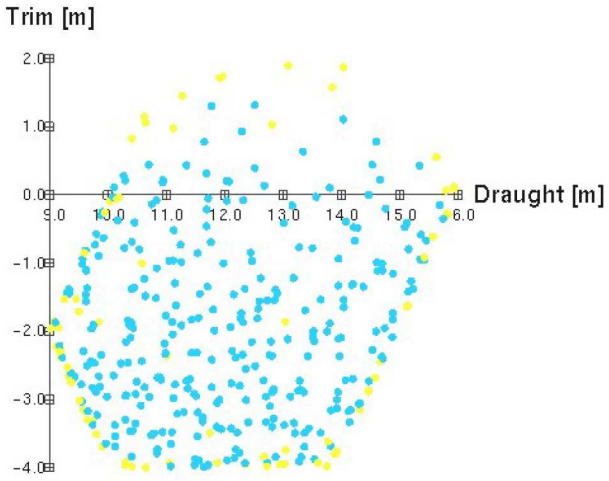

Figure 6. ULCV: distribution of loading conditions: trim versus draught-positive Trim by bow.

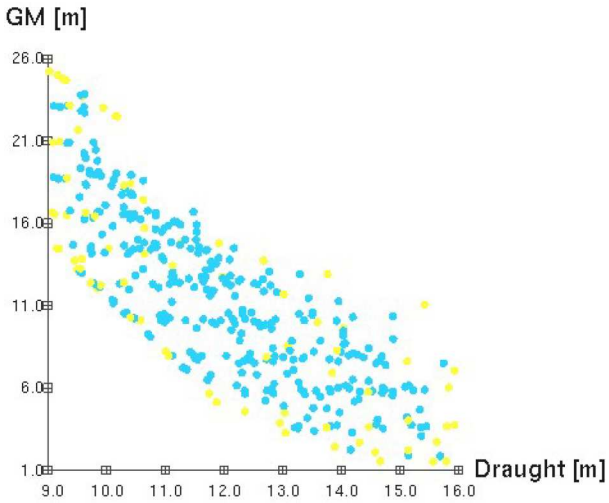

Figure 7. ULCV: distribution of loading conditions: GM versus draught.

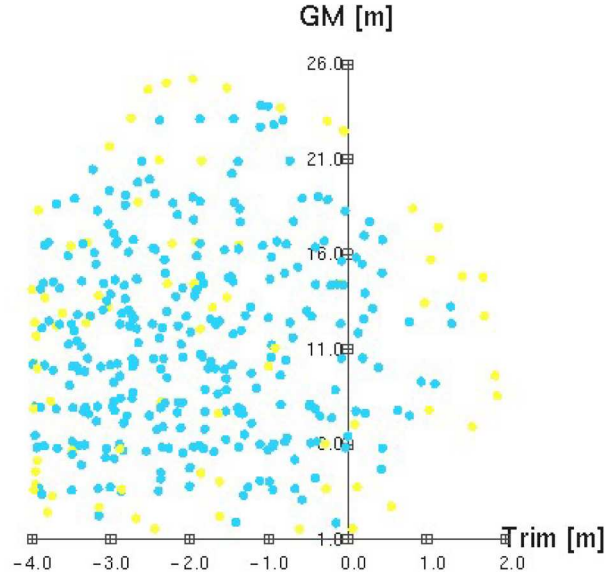

Figure 8. ULCV: distribution of loading conditions: GM versus trim-positive Trim by bow.

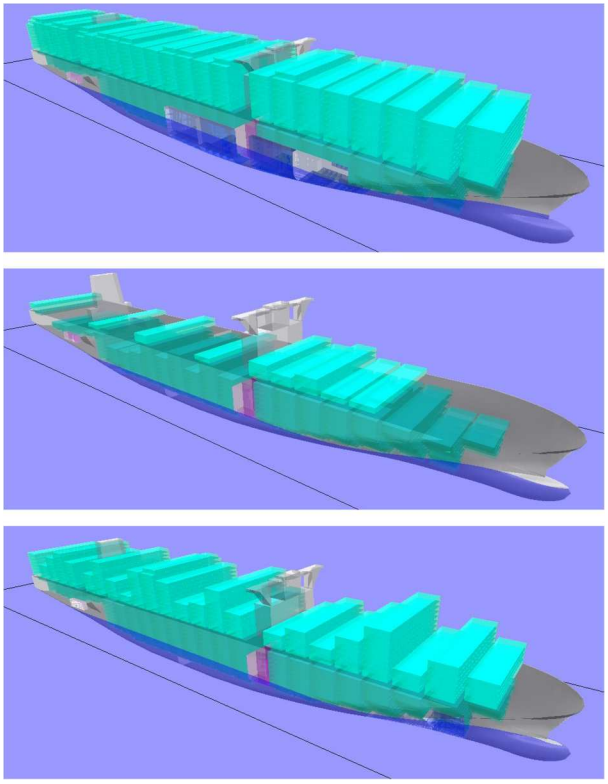

Figure 9. Example of loading conditions for an ultra large container vessel.

while the remaining blue points ly within this cloud. This distinction will be necessary in the further usage of these loading conditions by artificial intelligence. As a better display of the limits to the floating position, Figure 6 shows the distribution among trim and draught. The edges of this data cloud validate the before set limits to draughts and trim. In contrast, Figure 7 shows the distribution among metacentric height in draught. The lower edge of this resembles the curve of required minimum $\overline{GM}$. As can be seen $\overline{GM}$ may rise to excessive values for shallower draughts leading to strong lateral accelerations in seaway. This may be mitigated to some extent by using the uppermost ballast tanks in the ships sides. The remaining perspective showing the distribution among metacentric height and trim is pictured in Figure 8. There are no general limits in this context. However, it may be taken from this figure that $\overline{GM}$ is somewhat higher with sternwise trim. This observation is in line with the hydrostatics of the ship's

Table 2. Data of loading conditions shown in Figure 9.

LC		3 (top)	7 (middle)	10 (bottom)
T_{OX}	[m]	15.253	10.649	14.060
t	[m]	−0.993	0.413	−3.529
φ_{EQI}	[°]	0.967	0.413	0.371
$\overline{GM}_{EQI}$	[m]	3.350	15.577	5.883
Payload	[t]	158,863	89,722	153,841
Ballast	[t]	20,715	1391	1652
Consum.	[t]	5839	7258	8342
Δ	[t]	244,504	157,508	222,922
$k_{xx,dry}$	[m]	0.395 · B	0.308 · B	0.354 · B
n_{FEU}		9159	3703	7319

Table 3. RoRo vessel main particulars.

L_{OA}	≈190 m
B	≈26 m
D	≈17 m
LSW	≈8000 t
Δ_{SC}	≈22,000 t
L_{Lanes}	≈2700 m

Table 4. General cargo vessel main particulars.

L_{OA}	≈160 m
B	≈20 m
D	≈13 m
LSW	≈9000 t
Δ_{SC}	≈21,000 t
V_{Hold}	≈20,000 m^3

Table 5. Multi-role vessel main particulars.

L_{OA}	≈140 m
B	≈20 m
D	≈12 m
LSW	≈7000 t
Δ_{SC}	≈10,000 t
GT	≈12,000

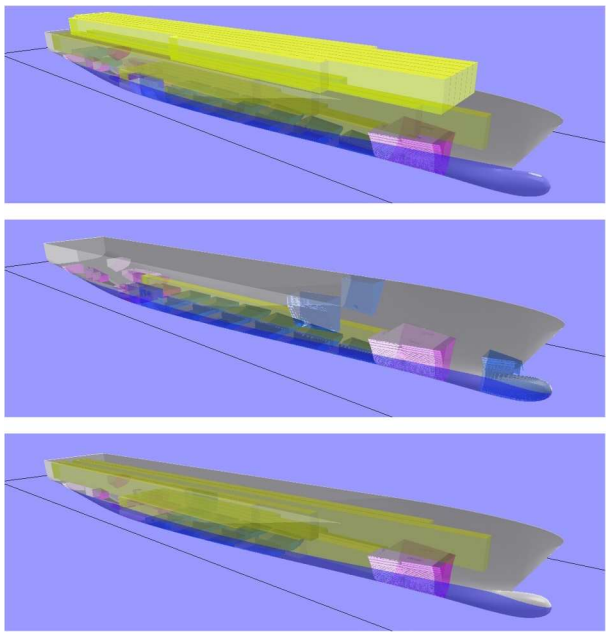

Figure 10. Example of loading conditions for an RoRo cargo vessel.

hull, since a sternwise trim submerges wider parts of the stern, therefore increasing the ships stability. Examples of loading conditions including their geometric arrangement of cargo, consumables and ballast are visualized in Figure 9 and their further details are listed in Table 2. Here the colour coding of individual components is equal to the one shown in Figure 1.

The application to a RoRo cargo vessel, a general cargo ship and a multi-role vessel, combining the described payload types, likewise shows plausible results. The main particulars of these vessels, as well as examples for drawn loading conditions are

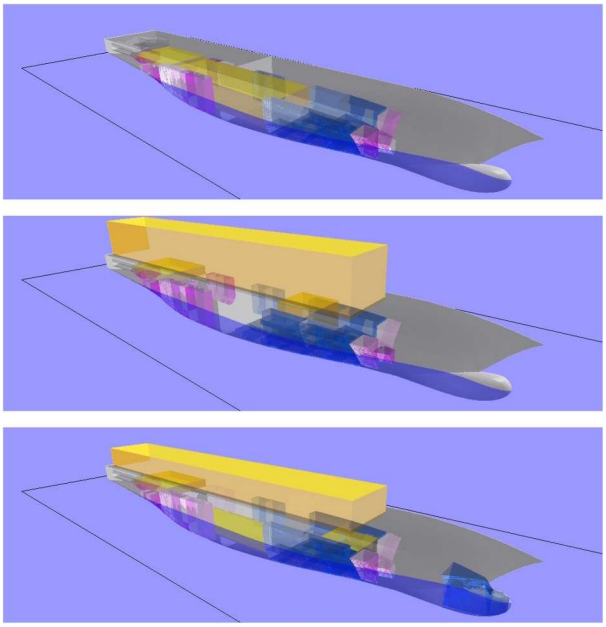

Figure 11. Example of loading conditions for a general cargo vessel.

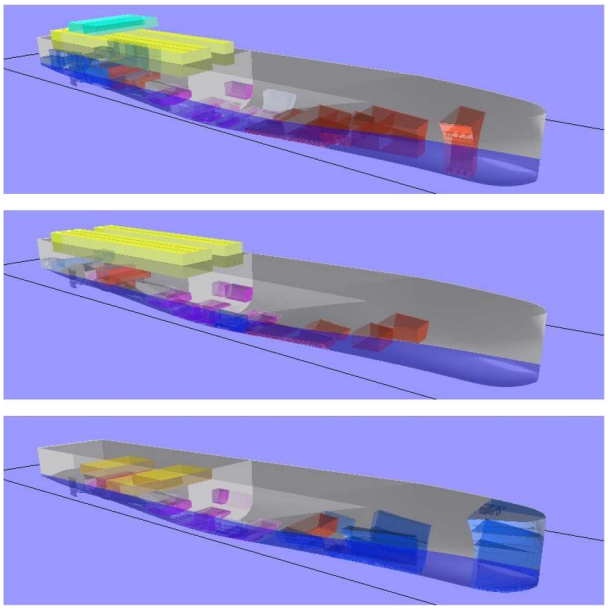

Figure 12. Example of loading conditions for a multi-role vessel.

documented in Tables 3–5 and Figures 10–12. Due to limited clearance of these vessels, no further data can be given about them.

5. Conclusion and outlook

From the results, it is concluded that the presented calculation process is capable of generating a sufficiently large distribution of loading conditions. It may therefore be used for in-depth analyses of the seakeeping behaviour. This may be done by computing physic-based training data for these loading conditions and generating a seakeeping model by utilizing artificial intelligence, as is documented in Krause and Krüger (2025a). Having a continuous model of the seakeeping behaviour may be used for different applications. It could be useful for comparing two ship designs against each other. Furthermore it may be utilized for route evaluation as will be documented in Krause and Krüger (2025b).

Disclosure statement

No potential conflict of interest was reported by the author(s).

References

Daewoo Shipbuilding & Marine Engineering Co., Ltd. 2015. H.NO 4279 – Trim and Stability Booklet.

Ghaemi H, Zeraatgar H. 2022. Impact of propeller emergence on hull, propeller, engine, and fuel consumption performance in regular head waves. Pol Marit Res. 29(4):56–76. doi: 10.2478/pomr-2022-0044

International Code on Intact Stability – 2020 Edition. 2020. London: International Maritime Organization.

Krause C. 2019. Operational guidance manual for an ultra large container vessel in different seaway conditions [Bachelor's thesis]. Hamburg: Hamburg University of Technology.

Krause C, Krüger S. 2025a. Prediction of extreme vessel responses utilizing artificial intelligence. In: Proceedings of the ASME 44th International Conference on Ocean, Offshore and Arctic Engineering, Vancouver, British Columbia, Canada. American Society of Mechanical Engineers.

Krause C, Krüger S. 2025b. Route evaluation on seakeeping risks using predictions by artificial intelligence. In: The 16th International Symposium on Practical Design of Ships and Other Floating Structures, Ann Arbor, Michigan, USA. University of Michigan.

Load Lines Convention 1966 – 2021 Edition. 2021. London: International Maritime Organization.

MARPOL CONSOLIDATED EDITION 2022. 2022. London.

Papanikolaou A. 2014. Ship design – methodologies of preliminary design. Springer.

SOLAS. 2020. Consolidated Edition 2020. London: International Maritime Organization.

Yasukawa H, Himaya A, Hirata N, Matsuda A. 2022. Simulation study of the effect of loading condition changes on the maneuverability of a container ship. J Mar Sci Technol. 28:98–116. doi: 10.1007/s00773-022-00908-3